



The superplastic forming/diffusion bonding and mechanical property of TA15 alloy for four-layer hollow structure with squad grid

Zhihao Du¹ · Kaifeng Zhang²

Received: 2 January 2021 / Accepted: 4 March 2021 / Published online: 15 March 2021
© The Author(s), under exclusive licence to Springer-Verlag France SAS, part of Springer Nature 2021

Abstract

The superplastic forming/diffusion bonding (SPF/DB) process has been widely applied to manufacture the multi-layer components. In this paper, a four-layer hollow structure with squad grid was fabricated by SPF/DB process. The superplastic behavior of TA15 alloy was investigated by the uni-axial tensile tests at high temperature, and the maximum elongation of 911 % was obtained at 920 °C/0.001 s⁻¹. The finite element method (FEM) of the four-layer structure was conducted, and the results showed that TA15 alloy was appropriate for fabricating this complex-shaped structure. Then the four-layer hollow structure was successfully fabricated by SPF/DB process at 920 °C with the target strain rate of 0.001 s⁻¹. Finally, the microstructure, thickness distribution and mechanical property of the four-layer hollow structure were investigated. The grain size increased from 5 μm to 10 μm and the sound bonding interface was achieved. The thickness distribution was symmetrical in height direction. The compressive strength and the maximum bending load of the four-layer hollow structure was 50 MPa and 64.4 kN, respectively.

Keywords SPF/DB · Four-layer hollow structure · TA15 alloy · FEM · Mechanical property

Introduction

Owing to the high specific strength, modest temperature strength, and good corrosion resistance, titanium alloy plays an important role in aerospace, nuclear, national defense and so on [1, 2]. The high deformation resistance and narrow range of deformation temperature made it difficult to process by conventional methods, while the difficulty could be overcome by the SPF/DB technology. SPF/DB process took advantage of the excellent superplasticity and diffusion bondability of titanium alloys [3–5]. It made the complex thin-wall parts integral and had great advantages in reducing structural weight and product costs [6–8]. Thus, it was necessary to investigate the SPF/DB process of titanium alloy.

TA15 alloy was widely used to manufacture structural components in aerospace due to its excellent properties at

elevated temperature [9, 10]. The high temperature deformation behavior and microstructure evolution of TA15 alloy were paid much attention [11–18]. Fan et al. [11] developed constitutive equation coupling microstructure evolution of TA15 titanium alloy. Zhao et al. [12] analyzed the microstructure evolution of TA15 titanium alloy subjected to equal channel angular pressing. Sun et al. [13] conducted the tensile tests to investigate the superplasticity of TA15 alloy and the maximum elongation value of 1074 % was obtained at the temperature of 900 °C and the strain rate of 3.3 × 10⁻⁴ s⁻¹. Ma et al. [14] studied the hot formability of TA15 titanium alloy sheet experimentally. Gao et al. [15] researched the flow behavior and microstructure evolution of TA15 alloy by isothermal compression test. Yang et al. [16] also employed the isothermal tensile tests and metallography examinations to investigate the flow softening and damage behavior in the hot forming of TA15 alloy. Zhao et al. [17] studied the deformation inhomogeneity and slip mode of polycrystalline TA15 titanium alloy sheets during the hot tensile process. Sun et al. [18] performed the hot compressive experiments of TA15 alloy to verify a microstructure evolution model.

Otherwise, Some researchers also studied the weldability of TA15 alloy with other materials [19–21] or itself [22, 23]. Li et al. [19] studied the diffusion bonding of TA15 and Ti₂AlNb alloys, and Zhang et al. [20] investigated the Laser

✉ Zhihao Du
duzhihaohit@126.com

¹ School of Mechanical and Electric Engineering, Nanyang Normal University, Nanyang 473061, China

² School of Materials Science and Engineering, Harbin Institute of Technology, Harbin 150001, China

TIG-hybrid-welding process of Ti-22Al-27Nb/TA15 dissimilar joints. The Laser beam welding to weld BTi-6431 S/TA15 titanium alloys was also researched by Zhang et al. [21]. Zhan et al. [22] and Wang et al. [23] investigated the laser beams welding process of TA15 alloy joints and tube, respectively.

Though some researchers investigated the SPD/DB process for four-layer structure of Ti-6Al-4 V alloy [24], Ti₂AlNb based alloy [25] and other materials [26], the research on the mechanical property of the multi-layer structure was few. While the structural strength was the critical demand for the application, so it was indispensable to investigate the mechanical properties of multi-layer structure.

In this study, the superplasticity of TA15 alloy at 920 °C was investigated. The FEM simulation of the process was carried out by the MSC.MARC software. The four-layer hollow structure with squad grid was fabricated by the SPF/DB technology. The microstructure was characterized. The thickness distribution of the structure at different regions was measured. And the compressive behavior and bending behavior of the structure were investigated at room temperature.

Experimental

The material used in this work was TA15 (Ti-6.5Al-2Zr-1Mo-1 V) alloy sheet with the thickness of 1.5 mm. The microstructure of as-received sheet and post-SPF/DB was observed by optical microscope, and the bonding interface microstructure was observed by scanning electron microscope (SEM) on a Quanta 200 FEG-SEM machine. The initial microstructure was shown in Fig. 1, and it consisted of the equiaxed fine grains. And the fine grain was significant for the SPF/DB process [27].

The tensile tests were carried out on an Instron 5500 machine with a heating furnace, and the strain rates were $1 \times 10^{-2} \text{ s}^{-1}$, $2.5 \times 10^{-3} \text{ s}^{-1}$, $1 \times 10^{-3} \text{ s}^{-1}$, and $3 \times 10^{-4} \text{ s}^{-1}$ at 920 °C. The tensile specimens with a gauge dimension of 15 mm×6 mm×1.5 mm were prepared by electro-discharge machining. The temperature was controlled within 2 °C along the

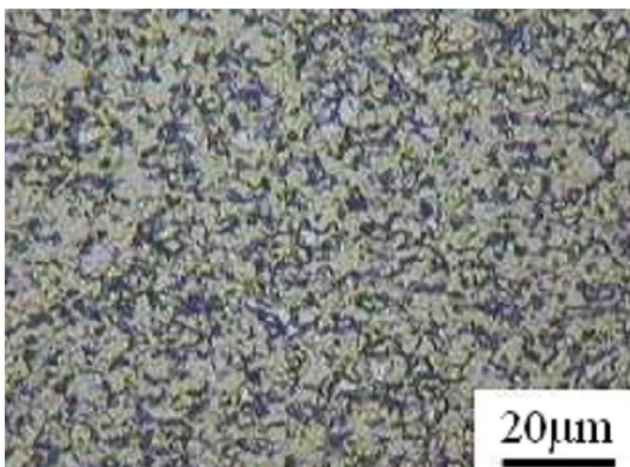


Fig. 1 The initial microstructure of TA15 alloy sheet

gauge length with the aid of three individual thermocouples. In order to guarantee the accuracy of tensile property, at least three tensile specimens were tested and the intermediate data at each condition was selected as the final result.

In order to fabricate the four-layer hollow structure, the SPF/DB process was conducted on the superplastic forming machine. The overall arrangement of four sheets made into a gas pack by peripheral sealing was illustrated in Fig. 2. The SPF/DB process was divided into two stages. The first stage was the diffusion bonding of two core sheets at bonding areas and the superplastic forming of two face sheets. The stop-off pattern was prepared on the core sheet surface, and it constructed the specific configuration of the hollow structure. The superplastic forming of core sheets, the diffusion bonding between core sheet and face sheet, and diffusion bonding between two core sheets at the stiffeners were the second stage. The argon gas was used in the SPF/DB process. The arrangement of stop-off pattern at core sheet surface and the finished hollow structure were shown in Fig. 3a and b, respectively.

The width of the DB joints between two core sheets, the thickness of the stiffeners and that of the two plates were measured. The micrometer was used. To ensure the accuracy of measurement, the dimension value at each point was measured at least three times, and the average value was regarded as the final value. The measured points and IDs were illustrated in Fig. 4.

The compressive behavior and bending behavior were investigated to evaluate the mechanical properties of the four-layer hollow structure. Samples for compression test and bending test were wire cut from the as-fabricated hollow structure. The specimens were cut at the middle part of the hollow structures. The specimens with the size of 80 mm×80 mm and the height of 18 mm were shown in Fig. 4. Four stiffeners with two longitudinal stiffeners and two transverse stiffeners were found, and the squad grid was formed by the longitudinal stiffener and the transverse stiffener. The span of two stiffeners was 38 mm.

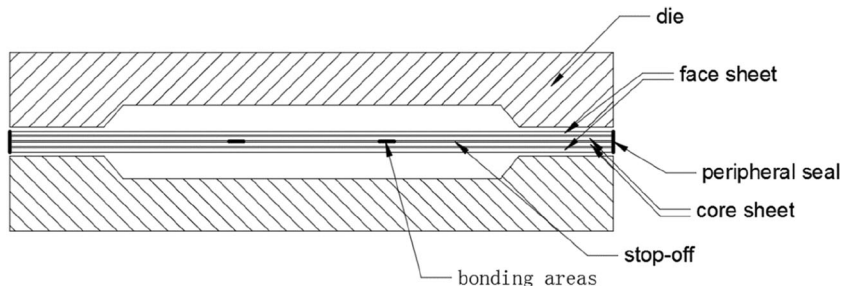
The compression test and bending test were conducted on the Instron 5569 machine, and the cross-speed was 2.0 mm/min. The schematic diagrams were illustrated in Fig. 5. In compression test, the specimen was put on the lower platform of the testing machine, and the upper surface contacted with the upper platform of the machine. In bending test, three 304 steel rods with the dimension of $\Phi 10 \text{ mm} \times 100 \text{ mm}$ were used.

Results and discussion

The superplasticity of TA15 alloy

The specimens and the true stress-strain curves of TA15 alloy at different strain rates with the temperature of 920 °C were

Fig. 2 the assembly prepared for SPF/DB process of the hollow structure



shown in Fig. 6. The flow stress was strongly sensitive to the strain rate. When the strain rate was 0.006 s^{-1} , the flow stress decreased to rupture after it reached the peak. And the true stress-strain curve was the typical softening curve. While the long strain hardening stages were observed at the strain rate of 0.001 s^{-1} and 0.0003 s^{-1} . This behavior might be an indication of grain growth which resulted from the long time exposure at high temperature. Then the grain growth caused the decrease of grain boundary length, and the difficulty of grain rotation or grain boundary sliding increased. This resulted in hardening. The physics of the flow stress curves could either be categorized in three or two distinctive stages [28, 29].

In addition, the saw-toothed shape was observed in the true stress-strain curves, and this phenomenon maybe resulted from the dynamic recrystallization or grain boundary sliding. And it showed that the increase or reduction of the flow stress was unexpected. The saw-toothed shape had been observed in other investigations [13, 30–32].

The influence of strain rate on the yield stress and the elongation was also shown in Fig. 7. The yield stress increased with the strain rate increasing. The elongation of 578 % was obtained at $920 \text{ }^\circ\text{C}/0.0003 \text{ s}^{-1}$. The elongation increased with the strain rate decreasing, and the maximum elongation was obtained at 0.001 s^{-1} , then it decreased when the strain rate was less than 0.001 s^{-1} . The long-time thermal exposure and the oxidation at 0.0003 s^{-1} led to the reduction. Additionally, the formation of a hard-brittle surface layer resulted from the oxidation diffusion on titanium [33–35] at high temperature also reduced the elongation. The maximum elongation of

911 % was achieved at $920 \text{ }^\circ\text{C}/0.001 \text{ s}^{-1}$, exhibiting excellent superplasticity.

During superplastic forming process, the forming temperature was constant, and the flow stress was sensitive to the strain rate [36]. The rigid plastic model was selected to describe the constitutive model, and the strain hardening co-exponent was neglected. The constitutive equation was established in power-law type [37] and expressed as:

$$\sigma = K \dot{\epsilon}^m$$

where m was the strain rate sensitivity coefficient, K was the material coefficient. On account of the flow stress curves in Fig. 6, the strain rate sensitivity coefficient m and the material coefficient K were computed to be 0.61 and $1030 \text{ MPa}\cdot\text{s}$, respectively.

The FEM simulation of the hollow structure with squad grid

In this study, a four-layer blade hollow structure was selected as the final component for TA15 alloy, owing to its excellent superplasticity. The FEM was used to simulate the SPF process and investigate the thickness distribution. The SPF process was also divided into two stages. The first stage was the SPF of the face sheet, and the second stage was the SPF of the core sheet. The FEM models for the SPF of the face sheet and the core sheet were shown in Fig. 8. The simplified models were constructed on account of the structural symmetry. The

Fig. 3 a The bonding areas of two core sheets; b the cross-section of the hollow structure

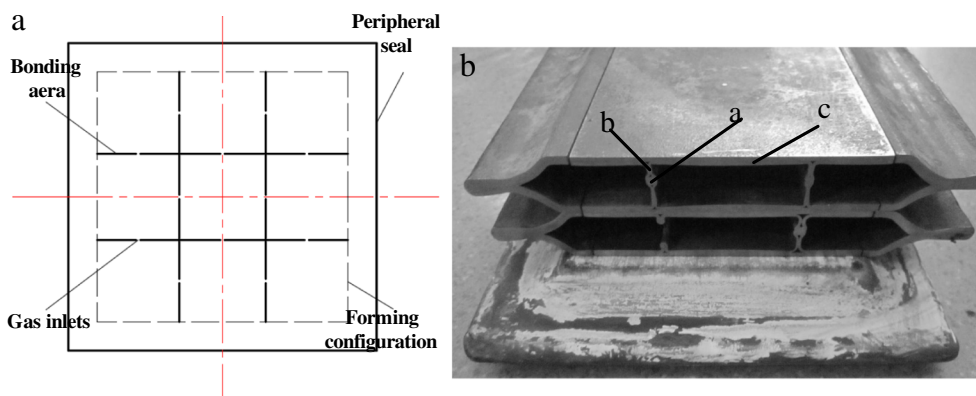


Fig. 4 The stiffeners' IDs, the measured points of stiffeners (a– width of joints; b– thickness of stiffeners near joints; c– thickness of stiffeners near plates) and that of two plates (-40 ~ 40)

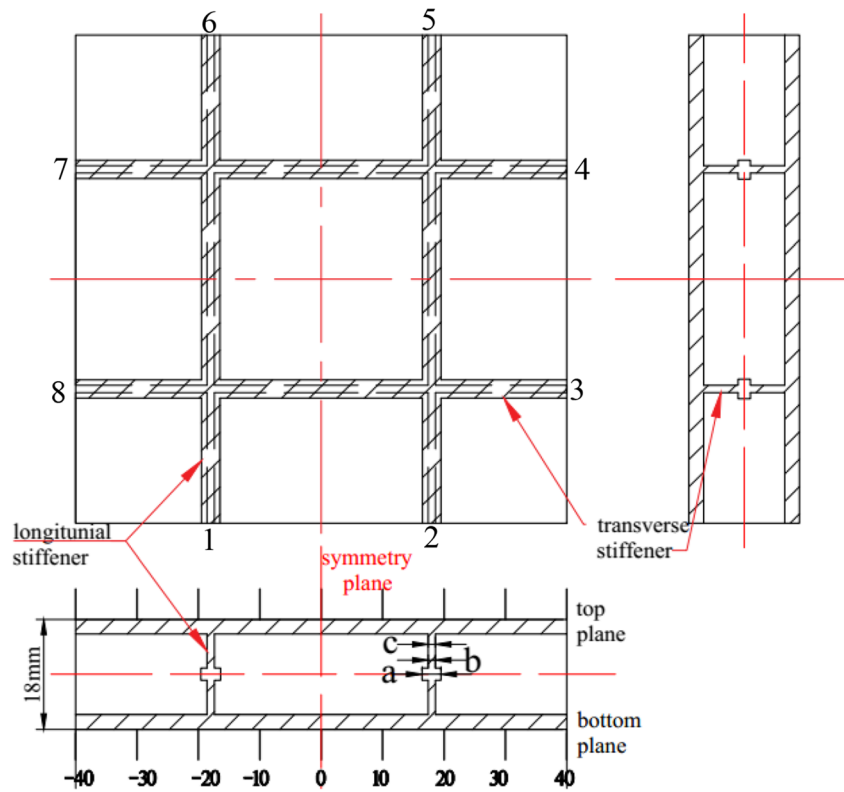


Fig. 5 The schematic diagram of mechanical property test: **a** a compression test; **b** bending test

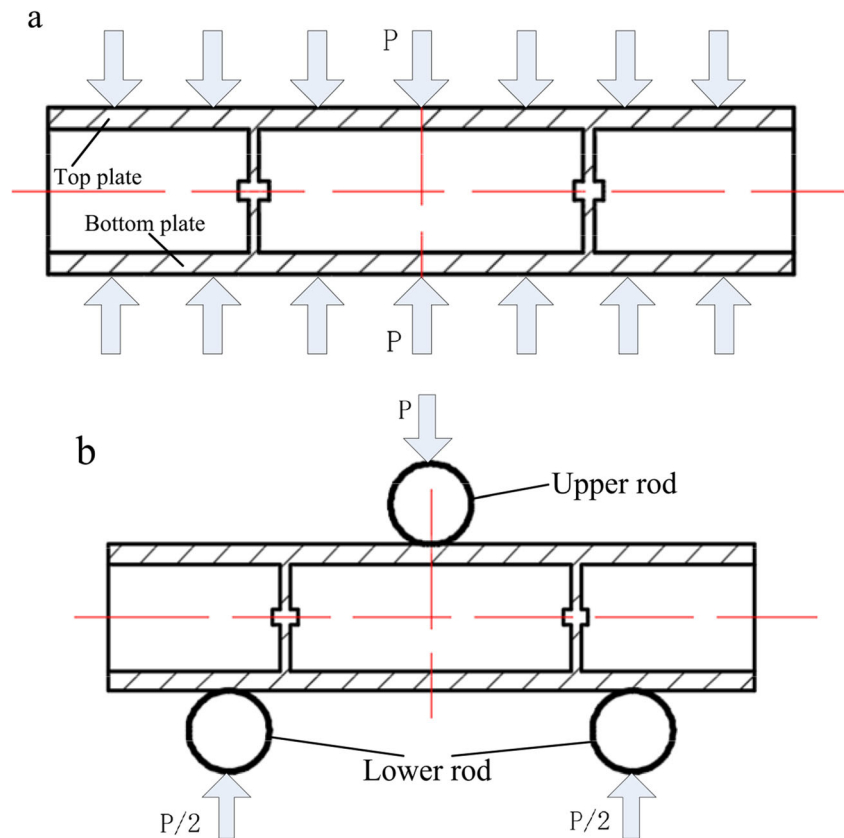
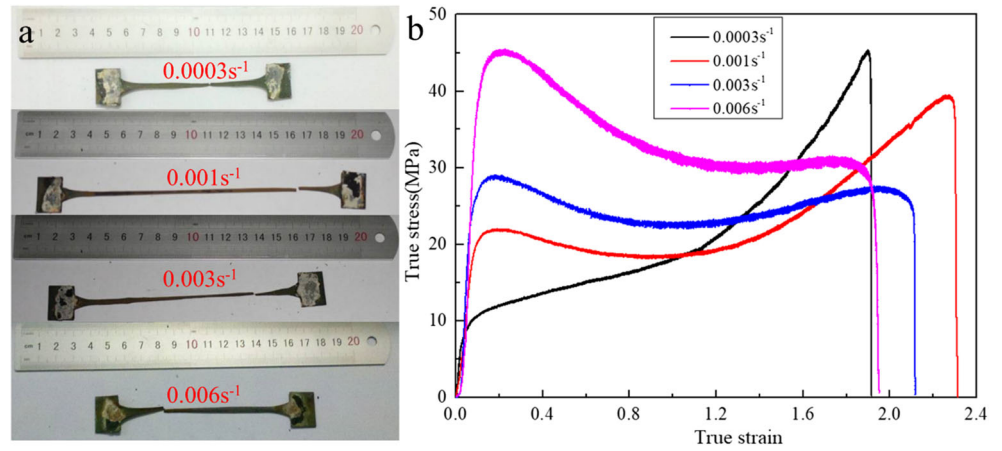


Fig. 6 **a** the tensile specimens and **b** the true stress-strain curves at 920 °C



half size of the sheets was 140 mm×70 mm. The four-node shell element with the size of 1 mm×1 mm was selected and the thickness was 1.5 mm. The width of bonding joints between two core sheets was 4 mm.

The above-mentioned constitutive equation was introduced into the FEM as the material property. The FEM simulation results of two sheets were shown in Fig. 9. Figure 9a showed the thickness distribution of the face sheet, and it was seen that the minimum thickness was 1.238 mm, and the difference of the thickness was less than 0.3 mm. The thinning ratio of the face sheet was less than 18 %. Figure 9b showed the thickness curve of the symmetry line with arc length varying from 0 to 140 at the face sheet. The minimum thickness took place at the transition fillet and it was about 1.35 mm.

The FEM result of the core sheet was shown in Fig. 9c. And Fig. 9d showed the thickness curve of the symmetry line with arc length varying from 0 to 140 at the core sheet. The thickness distribution of core sheet at different regions was seriously inhomogeneous. The material near the bonding joint gradually erected and contacted closely together to bond with each other and form the stiffers in the forming process. The deformation of the core sheet was similar with that of the

multi-rectangular box and it was seriously different at different regions. The minimum thickness occurred at the top of the vertical stiffeners in Fig. 9c and it was 0.595 mm. The deformation of the whole vertical stiffeners was serious and the thickness distribution ranged from 0.6 mm to 0.7 mm in Fig. 9d. It was seen that the thinning mainly focused on the vertical stiffeners. The maximum thinning ratio of the core sheet was appropriately about 60 %. The excellent superplasticity of TA15 alloy could meet this requirement, and it could be concluded that the SPF/DB process was feasible for fabricating this blade hollow structure.

The SPF/DB of TA15 alloy

The SPF/DB process was carried out to fabricate the hollow structure on the superplastic forming machine. The temperature was set to be 920 °C, and it was kept for about 0.5 h to make the temperature homogeneous, then the SPF of the face sheet started. In order to keep the target strain rate of the deformation retaining at 0.001 s⁻¹, the pressure-time curves of the SPF process for the face sheet and the core sheet were generated by the FEM simulation. During the SPF/DB process of TA15 alloy, the pressure-time curves were shown in Fig. 10. The modified pressure-time curves were optimized based on the pressure-time curves of FEM simulation. And the modified pressure-time curves were applied at the beginning of the two stages.

It has been investigated that the diffusion bonding of TA15 alloy at 2.0 MPa/1.5 h could achieve the sound bonding joint [38]. The maximum gas pressure of the SPF/DB process was 2.0 MPa to guarantee the achievement of the sound joint. When the SPF of the face sheet or the core sheet completed, the gas pressure gradually increased to 2.0 MPa and the DB process started. The pressure of 2.0 MPa was kept for 1.5 h at the first stage. At the second stage, the increase of the pressure in experiment was slightly slower than the modified pressure so as to release the crack of bonding joints. Figure 3b showed the cross-section of the final blade hollow structure with squad

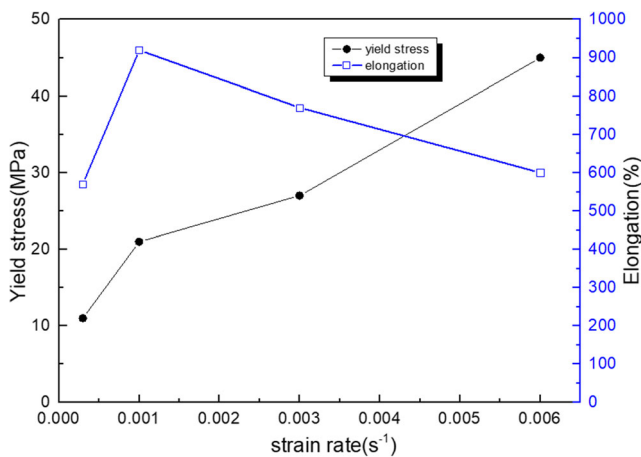


Fig. 7 The variation of tensile stress, and elongation at different strain rates

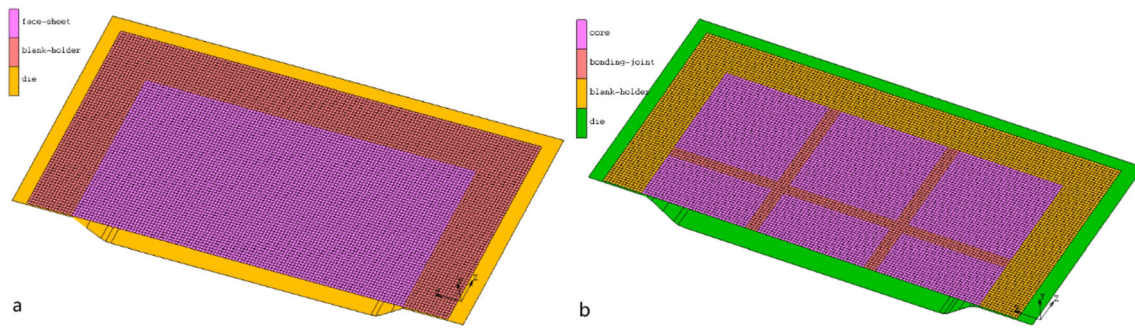


Fig. 8 The simplified FEM model for the SPF process of (a) face sheet; (b) core sheet

grid. It was seen that the forming quality of this hollow structure was good and the accurate configuration was obtained.

Microstructure

The microstructure of the post-SPF/DB material was shown in Fig. 11. Compared with the initial microstructure in Fig. 1, it was seen that the grain size increased remarkably from 5 μm to 10 μm . In order to make the deformation and diffusion sufficient, the material experienced high temperature for a long time, which resulted in the grain growth.

Figure 12 showed the microstructure of the bonding interfaces at the corresponding regions in Fig. 3b. The interfacial

microstructure of the bonding joint between two core sheets, and that of the stiffener and the bonding region between core and face sheet were represented in Fig. 12a, b, c, respectively.

During the SPF/DB process, the bonding interface of the selective bonding areas between two core sheets influenced the forming of the squad grids at the second stage. No defect was observed at the bonding area in Fig. 12a, and it could be concluded that the DB was complete and the sound bonding joints were achieved at the first stage. And this result also showed that TA15 alloy possessed excellent bondability. The interfacial microstructure of the stiffener and that of the bonding region between core sheet and face sheet were shown in Fig. 12b and c, respectively. Some discontinuing voids

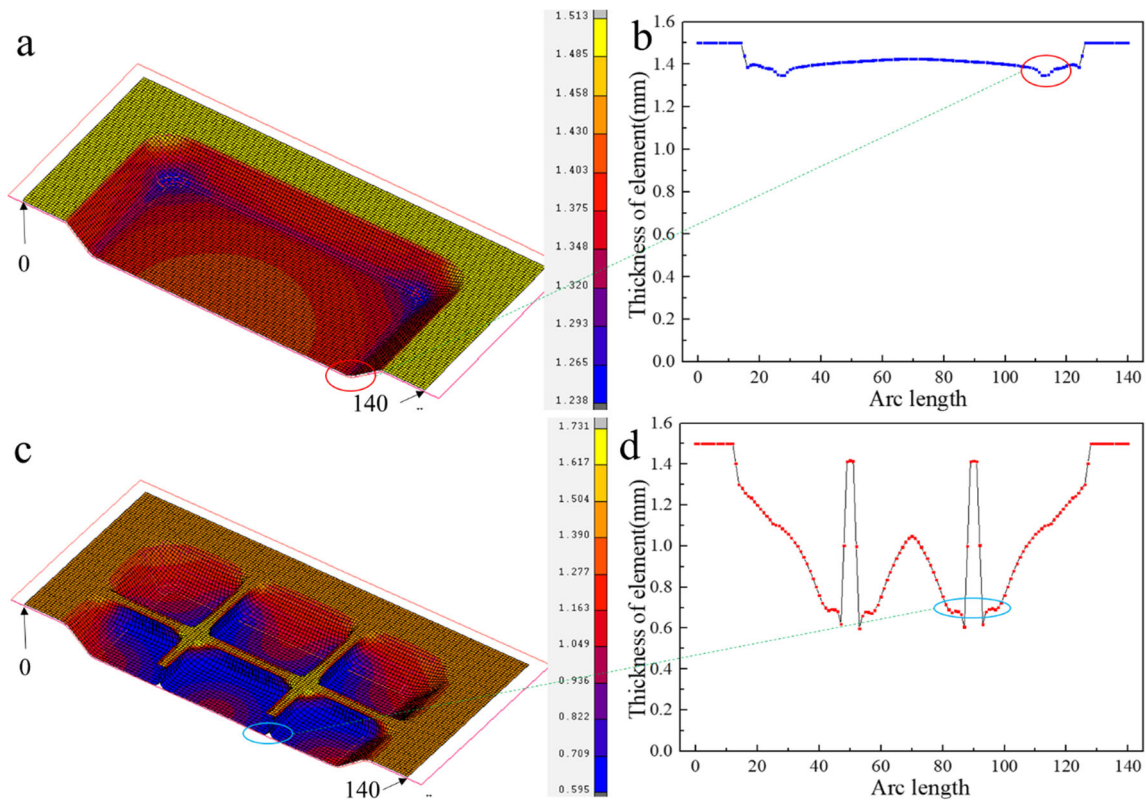
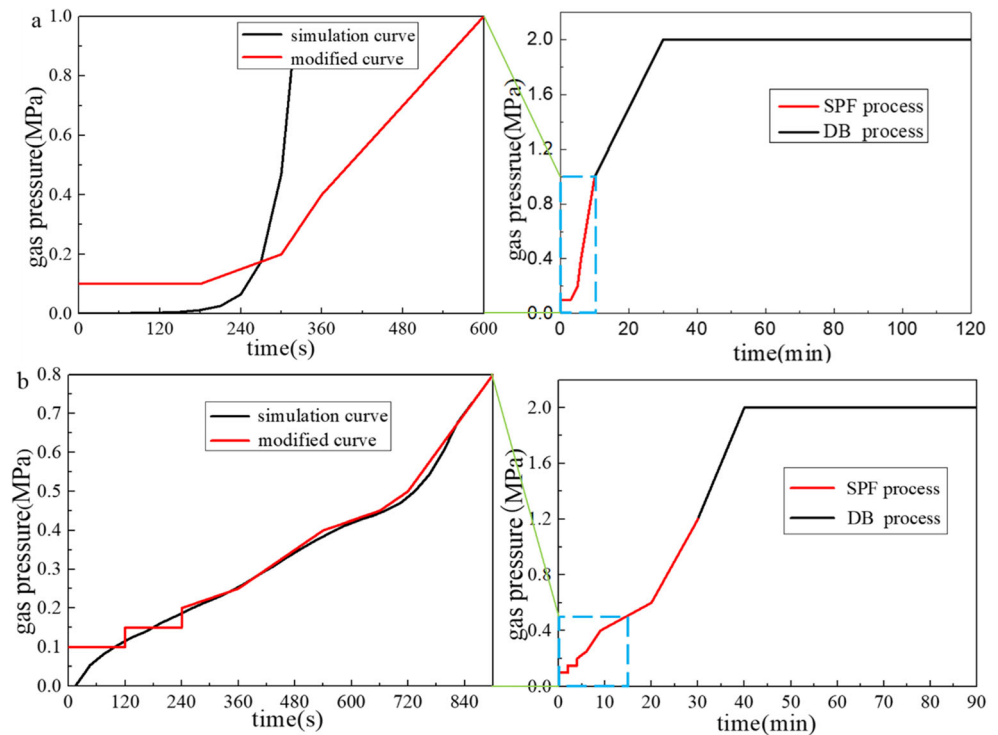


Fig. 9 The thickness distribution of (a) face sheet; (b) the line at face sheet with arc length varying from 0 to 140; (c) core sheet; (d) the line at core sheet with arc length varying from 0 to 140;

Fig. 10 The pressure-time curves of (a) the first stage; (b) the second stage



were observed at the interface, and it resulted from the insufficient DB for short time. And these voids would disappear with the bonding time increasing.

Thickness distribution

Given the strength requirement of the structure, the thickness distribution of SPF/DB structure must be investigated. And the thickness at different regions of the hollow structure was shown in Fig. 13.

The bonding joints' width and the thickness distribution of the different stiffeners were almost uniform in Fig. 13a, while

the thickness of the same stiffener at different regions was still different. The width of the bonding joints was preset as 4.0mm, and the measured width varied from 2.48 mm to 3.06 mm. It was indicated that the bonding width decreased at the second stage and the maximum reduction was almost 37.5 %. Although the minimum width of joints was less than 3.0 mm, it was still larger than the thickness of stiffeners, which made the width reduction of bonding joints had little influence on the reinforcement of the stiffeners. The thickness of the stiffeners near the joints was about 1.0 mm and the maximum thickness difference was 0.2 mm. The thickness of these stiffeners near the plate was about 1.25 mm and the maximum difference was 0.4mm. The thickness reduction near joints was more severe than that near the plate. And it was consistent with the results of the FEM simulation.

The thickness of the top and bottom plates was about 2.3 mm and the maximum thickness difference was 0.42 mm in Fig. 13b. The thickness of the regions at the middle of the squad grid were larger than that of the regions near stiffeners which were about ± 18 mm away from the middle symmetry plate.

The thickness distribution was related to the order of the core sheet contacting with the face sheet. The deformation of core sheet firstly occurred at the middle part of the squad grids, and the thickness of this part would not change when the core sheet contacted with the face sheet due to friction. Then the deformation began to take place at the parts near stiffeners and it was so serious that the thickness of this part became the minimum value. It was also shown that the thickness of the top plate and the bottom plate at the corresponding positions

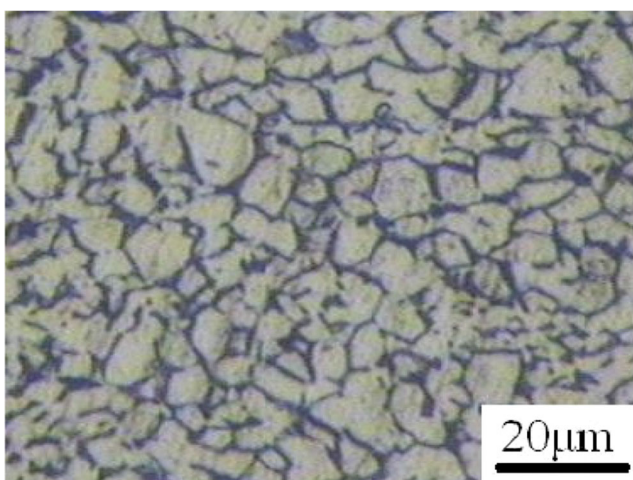
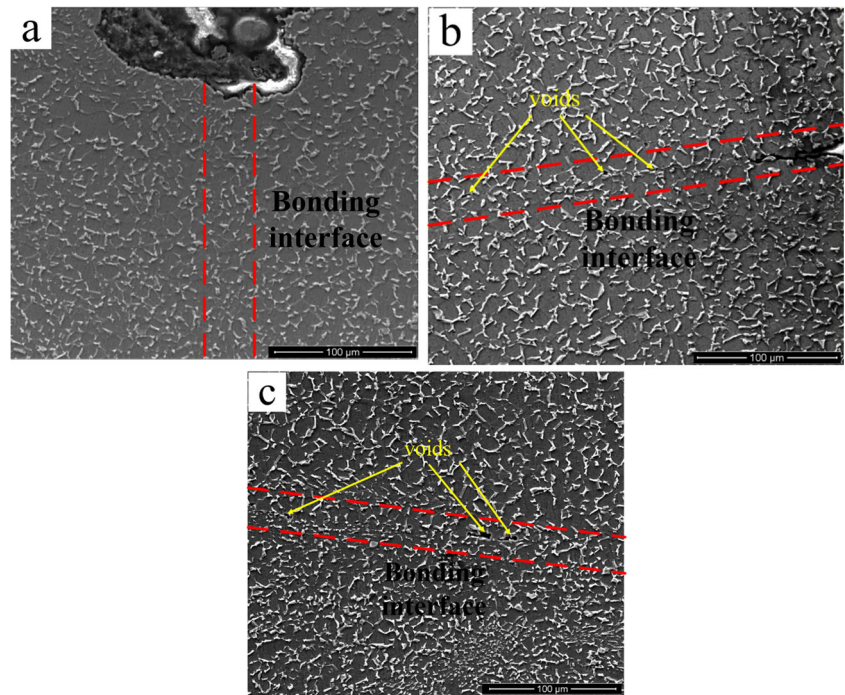


Fig. 11 The microstructure of post-SPF/DB material

Fig. 12 Interfacial microstructure of: **a** bonding joint between two core sheets; **b** stiffener; **c** bonding region between core and face sheet



was basically equal, and the maximum thickness difference was only 0.14 mm. And the thickness distribution was symmetrical to the middle plate in height direction.

Mechanical property tests

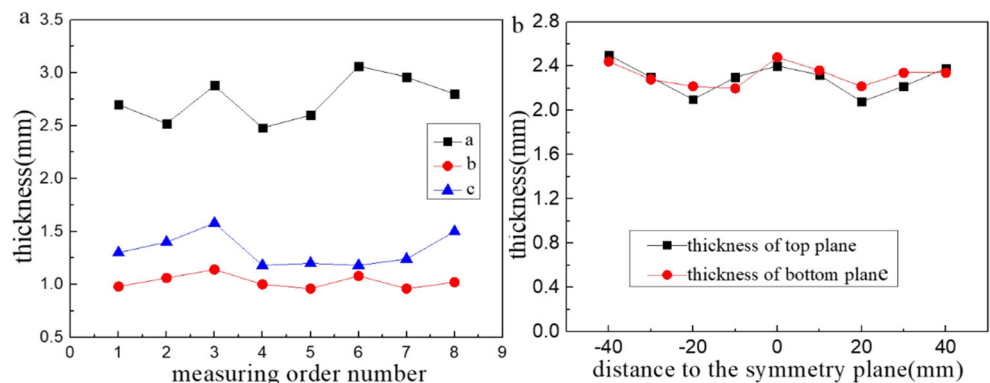
The thickness distribution and the microstructure evolution were investigated, thus, the critical demands on the structural strength of the structure had been determined. It was necessary to carry out the operation experimental tests for confirming the applicability. Thus, the compression test and bending test were conducted to investigate the mechanical property of the hollow structure.

Compression test The load-bearing capacity was measured to evaluate the mechanical property of the structure. The compression stress-displacement curve was shown in Fig. 14, and

the compressive stress was calculated from the planar area of the hollow sample. The compressive behavior of this four-sheet structure was studied and the deformation after instability didn't need to be researched, so the load stopped when the specimen began to be instability. The compressive stress increased with the increase of the displacement until it reached up to the maximum value. The maximum compressive stress reached up to 50 MPa when the displacement value was about 1.9mm. Then the compression stress started to decline.

Bending test The load-displacement curve of this structure in the bending test was shown in Fig. 15. The load increased rapidly at the initial stage of the bending test, then began to increase gradually with the displacement increasing. The load reached the maximum value of 64.4 kN at the displacement of 2.75 mm and it changed slightly until the displacement up to

Fig. 13 Thickness distribution of (a) stiffeners; (b) top and bottom plates



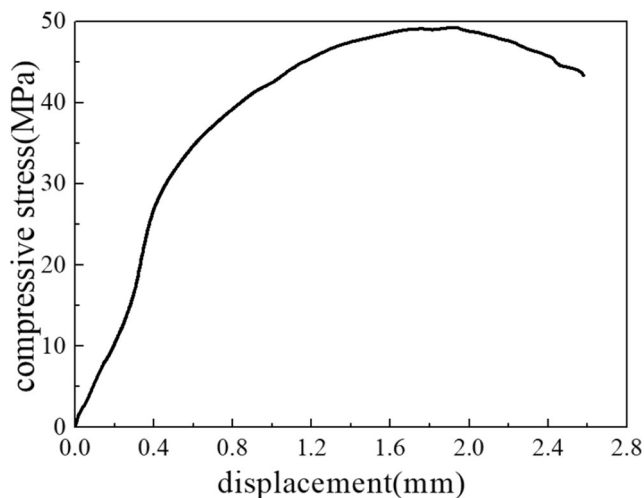


Fig. 14 Compressive stress-displacement curve

3.0 mm. Then the load decreased and the minimum load was about 60 kN. The bending load changed a little with the displacement varying from 3.0 mm to 6.0 mm.

Conclusions

The mechanical property and microstructure evolution of TA15 alloy for the four-layer hollow structure were investigated, and the following conclusions were drawn from this investigation:

- (1) The four-layer hollow structure of TA15 alloy was successfully fabricated by SPF/DB process, indicating that this process was appropriate for manufacturing this hollow structure.
- (2) The grain growth was obvious due to the long time thermal exposure. The width of bonding joints decreased and the sound bonding joints were achieved.

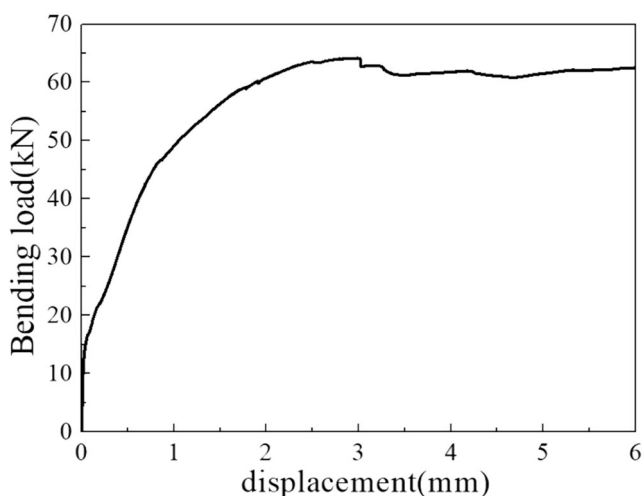


Fig. 15 Load-bearing curve of bending test

- (3) The thickness of the stiffeners near joints was less than that of the stiffeners near plates and the thickness distribution of the top plate and the bottom plate was symmetrical in height direction.
- (4) The maximum compressive strength of the specimen was 50 MPa and the maximum bending load was 64.4 kN in bending test.

Acknowledgements This work was supported by Henan Provincial Department of Science and Technology Research Project (Grant No. 182102210468).

Declarations

Conflict of interest The authors declare that they have no conflict of interest.

References

1. Bathini U, Srivatsan TS, Patnaik A, Quick T (2010) A study of the tensile deformation and fracture behavior of commercially pure Titanium and Titanium alloy: influence of orientation and microstructure. *J Mater Eng Perform* 19:1172–1182
2. Orhan N, Khan TI (2001) Diffusion bonding of a micro duplex stainless to Ti-6Al-4V. *Scripta Mater* 45(4):441–446
3. Xun YW, Tan MJ (2000) Applications of superplastic forming and diffusion bonding to hollow engine blades. *J Mater Process Technol* 99:80–85
4. Hefti LD (2010) Fine-grain titanium 6Al-4V for superplastic forming and diffusion bonding of aerospace products. *JOM* 62(5): 42–45
5. Kaibyshev OA, Safiullin RV, Lutfullin RY, Valiakhmetov OR, Galeev RM, Dutta A, Raghu T, Saha GG (2006) Advanced superplastic forming and diffusion bonding of titanium alloy. *Mater Sci Technol* 22(3):343–348
6. Jiang SS, Jia Y, Lu Z, Shi CC, Zhang KF (2017) Superplastic forming/diffusion bonding without interlayer of 5A90 Al-Li alloy hollow double-layer structure. *J Mater Eng Perform* 26:4265–4273
7. Xing HL, Wang CW, Zhang KF, Wang ZR (2004) Recent development in the mechanics of superplasticity and its applications. *J Mater Process Technol* 151:196–202
8. Mikhaylovskaya AV, Mosleh AO, Kotov AD, Kwame JS, Pourcelot T, Golovin IS, Portnoy VK (2017) Superplastic deformation behaviour and microstructure evolution of near- α Ti-Al-Mn alloy. *Mater Sci Eng A* 708:469–477
9. Peters M, Kumpfert J, Ward CH, Leyens C (2010) Titanium alloys for aerospace applications. *Adv Eng Mater* 5(5):419–427
10. Zhao ZL, Guo HZ, Chen L, Yao ZK (2009) Superplastic behaviour and microstructure evolution of a fine-grained TA15 Titanium alloy. *Rare Met* 28(5):523–527
11. Fan XG, Yang H, Gao PF (2013) Prediction of constitutive behavior and microstructure evolution in hot deformation of TA15 titanium alloy. *Mater Des* 51:34–42
12. Zhao Y, Guo HZ, Shi ZF, Yao ZK, Zhang YQ (2011) Microstructure evolution of TA15 titanium alloy subjected to equal channel angular pressing and subsequent annealing at various temperatures. *J Mater Process Technol* 211:1364–1371
13. Sun QJ, Wang GC (2014) Microstructure and superplasticity of TA15 alloy. *Mater Sci Eng A* 606:401–408

14. Ma BL, Wu XD, Li XJ, Wan M, Cai ZY (2016) Investigation on the hot formability of TA15 titanium alloy sheet. *Mater Des* 94:9–16
15. Gao PF, Zhan M, Fan XG, Lei ZN, Cai Y (2017) Hot deformation behavior and microstructure evolution of TA15 titanium alloy with nonuniform microstructure. *Mater Sci Eng A* 689:243–251
16. Yang L, Wang BY, Liu G, Zhao HJ, Xiao WC (2015) Behavior and modeling of flow softening and ductile damage evolution in hot forming of TA15 alloy sheets. *Materials Design* 85:135–148
17. Zhao J, Lv LX, Liu G, Wang KH (2017) Analysis of deformation inhomogeneity and slip mode of TA15 titanium alloy sheets during the hot tensile process based on crystal plasticity model. *Mater Sci Eng A* 707:30–39
18. Sun ZC, Yang H, Han GJ, Fan XG (2010) A numerical model based on internal-state-variable method for the microstructure evolution during hot-working process of TA15 titanium alloy. *Mater Sci Eng A* 527:3464–3471
19. Li P, Ji XH, Xue KM (2017) Diffusion bonding of TA15 and Ti₂AlNb alloys: interfacial microstructure and mechanical properties. *J Mater Eng Perform* 26:1839–1846
20. Zhang KZ, Lei ZL, Chen YB, Liu M, Liu Y (2015) Microstructure characteristics and mechanical properties of laser-TIG hybrid welded dissimilar joints of Ti-22Al-27Nb and TA15. *Opt Laser Technol* 73:139–145
21. Zhang H, Hu SS, She JQ, Li DL, Bu XZ (2015) Effect of laser beam offset on microstructure and mechanical properties of pulsed laser welded BTi-6431S/TA15 dissimilar titanium alloys. *Opt Laser Technol* 74:158–166
22. Wang KH, Liu G, Zhao J, Wang JL, Yuan SJ (2016) Formability and microstructure evolution for hot gas forming of laser-welded TA15 Titanium alloy tube. *Mater Des* 91:269–277
23. Zhan XH, Peng QY, Wei YH, Ou WM (2017) Experimental and simulation study on the microstructure of TA15 titanium alloy laser beam welded joints. *Opt Laser Technol* 94:279–289
24. Han WB, Zhang KF, Wang GF (2007) Superplastic forming and diffusion bonding for honeycomb structure of Ti-6Al-4V alloy. *J Mater Process Technol* 183(2–3):450–454
25. Du ZH, Jiang SS, Zhang KF, Lu Z, Li BY, Zhang DL (2016) The structural design and superplastic forming/diffusion bonding of Ti₂AlNb based alloy for four-layer structure. *Mater Des* 104:242–250
26. Sanders DG, Ramulu M (2004) Examination of superplastic forming combined with diffusion bonding for Titanium: perspective from experience. *J Mater Eng Perform* 13:744–752
27. Sherby OD, Wadsworth J, Caligiuri RD, Eiselstein LE, Snyder BC, Whalen RT (1979) Superplastic bonding of ferrous laminates. *Scr Metall* 13:941–946
28. Yasmeeen T, Shao ZT, Zhao L, Gao P, Lin JG, Jiang J (2019) Constitutive modelling for the simulation of the superplastic forming of TA15 Titanium alloy. *Int J Mech Sci* 164:105178
29. Yasmeeen T, Zhao B, Zheng JH, Tian F, Lin J, Jiang J (2020) The study of flow behavior and governing mechanisms of a titanium alloy during superplastic forming. *Mater Sci Eng A* 788:139482
30. Sergueeva AV, Stolyarov VV, Valiev RZ, Mukherjee AK (2000) Enhanced superplasticity in a Ti-6Al-4V alloy processed by severe plastic deformation. *Scr Mater* 43:819–824
31. Huang BY, Zhang JH, He YH, Liu Y, Sun J, Wu JS (2002) Superplastic behavior of TiAl based alloy at relatively low temperatures ranging from 800°C to 1075°C. *Trans Nonferrous Met Soc China* 12(4):577–581
32. Jia JB, Zhang KF, Liu LM, Wu FY (2014) Hot deformation behavior and processing map of a powder metallurgy Ti-22Al-25Nb alloy. *J Alloy Compd* 600:215–221
33. Yue LY, Wang ZB, Li L (2012) Material morphological characteristics in laser ablation of alpha case from titanium alloy. *Appl Surf Sci* 258:8065–8071
34. Chen GZ, Fray DJ, Farthing TW (2001) Cathodic deoxygenation of the alpha case on titanium and alloys in molten calcium chloride. *Metall Mater Trans B* 32:1041–1052
35. Sung SY, Kim YJ (2005) Alpha-case formation mechanism on titanium investment castings. *Mater Sci Eng A* 405:173–177
36. Zhang TY, Liu Y, Sanders DG, Liu B, Zhang WD, Zhou CX (2014) Development of fine grain size titanium 6Al-4V alloy sheet material for low temperature superplastic forming. *Mater Sci Eng A* 608:265–272
37. Cheng JH (1996) The determination of material parameters from superplastic inflation tests. *J Mater Process Technol* 58:233–246
38. Liu JJ, Fu MJ, Xu HY, Han XQ, Shao CL (2016) Superplasticity and diffusion bonding property of TA15 alloy. *J Plast Eng* 23(6): 73–178

Publisher's note Springer Nature remains neutral with regard to jurisdictional claims in published maps and institutional affiliations.